University of Alberta

Deposition and Characterization of Thin Alumina Films Grown by Electron Beam Evaporation

by

Harun Muhammed

A thesis submitted to the Faculty of Graduate Studies and Research

in partial fulfillment of the requirements for the degree of

Master of Science

in

Materials Engineering

Department of Chemical and Materials Engineering

©Harun Muhammed

Spring 2011

Edmonton, Alberta

Permission is hereby granted to the University of Alberta Libraries to reproduce single copies of this thesis and to lend or sell such copies for private, scholarly or scientific research purposes only. Where the thesis is converted to, or otherwise made available in digital form, the University of Alberta will advise potential users of the thesis of these terms.

The author reserves all other publication and other rights in association with the copyright in the thesis and, except as herein before provided, neither the thesis nor any substantial portion thereof may be printed or otherwise reproduced in any material form whatsoever without the author's prior written permission.

EXAMINING COMMITTEE

Dr. Kenneth Cadien, Chemical and Materials Engineering

Dr. David Mitlin, Chemical and Materials Engineering

Dr. Douglas Barlage, Electrical and Computer Engineering

ABSTRACT

In thin film fabrication, growth of high quality thin films with reproducibile properties is one of the main challenges. In order to achieve this goal, the influnce of the deposition system control parameters on film properties must be studied. This can be a complex process since many parameters may need to be considered. In this thesis, the electron beam evaporation of thin aluminum oxide films was investigated. Films were deposited with and without oxygen supply in the chamber, and at various ebeam source settings. A Varialble Angle Spectroscopic Ellipsometry system was used to characterize the films. Refractive index, which depends on material density and stoichiometry, was used as the figure of merit. It was observed that refractive index increases with deposition rate. Refractive index also changes with oxygen pressure and upon exposure to air. Various models to explain this behaviour are proposed and discussed.

ACKNOWLEDGEMENTS

I would like to express my deepest gratitude to my supervisor Dr. Kenneth Cadien for his continuous support and guidance during my involvement with the whole project. I express my sincere appreciation for his approach toward students that must have a positive impact in my future life. Many good things could happen at a time if there is proper approach and support. Things might have been different if it were not Dr. Cadien.

I would like to extend my thanks to Dr. Ellezzabi, from Electrical Engineering department, for his support for the project. I take pleasure to thank Les Schowalter and Scott Munro for their support and letting me access tools 24/7 in Nanofab lab. My special thanks to my former fellow colleague Wei Guo for her suggestions throughout the project. I remember the nice friendly environment among colleagues in Dr. Cadien's research group. I would like to thank all the people I have had contact with and got help throughout the project.

At last I remember my parents and brothers and sisters for unconditional supports that helped me come to this position today.

TABLE OF CONTENTS

1. INTRODUCTION 1

1.1 Background 1

1.2 Organization of Thesis 2

2. LITERATURE REVIEW 3

2.1 Thin Film Aluminum Oxide 3

2.2 Aluminum Oxide Deposition by Electron Beam Evaporation 5

2.2.1 Aluminum Oxide from Source Al with Oxygen Gas 5

2.2.2 Aluminum Oxide from Source Alumina 9

3. ELECTRON BEAM DEPOSITION SYSTEM AND CONTROL PARAMETERS 16

3.1 Electron Beam Evaporation System 16

3.2 Control Parameters 17

3.2.1 Acceleration Voltage 18

3.2.2 Beam Current 20

3.2.3 Sweep Area 20

3.2.4 Source to Substrate Distance 21

3.2.5 Substrate Temperature 22

3.2.6 Chamber Pressure 22

3.2.7 Crucible and Water Cooling 23

4. EXPERIMENTAL PROCEDURE 25

4.1 Sample Preparation..25
4.1.1 Wafer Cleaning 25
4.1.2 Native Oxide Thickness Measurement 27
4.2 Film Deposition 27
4.3 Film Characterization 33
5. RESULTS AND DISCUSSIONS 36
5.1 Optical Characterization 36
5.1.1 General Modeling...36
5.1.2 Cauchy Modeling 39
5.2 Influence of Deposition Variables 42
6. CONCLUSIONS AND FUTURE WORK 52
6.1 Conclusions 52
6.2 Future work...53
References 55

LIST OF TABLES

Table 4-1 Deposition Parameters 33

Table 5-1 VASE Modeling Parameters 41

Table 5-2 Sample Thickness 41

LIST OF FIGURES

Figure 2-1 Alumina dispersion curve comparison deposited by different deposition techniques 11

Figure 3-1 Schematic diagram of electron beam evaporation system ....
.... 17

Figure 3-2 Electron beam interactions with target 19

Figure 4-1 Electron beam deposition system used in the project 28

Figure 4-2 Used alumina source grains in coated graphite crucible 30

Figure 4-3 Schematic diagram of ellipsometry working process 34

Figure 4-4 VASE system used from J. A. Woollom Co., Inc. 35

Figure 5-1 VASE model and actual sample layers arrangement without roughness considered 37

Figure 5-2 VASE model and actual sample layers arrangement with roughness considered 37

Figure 5-3 MSE comparison between roughness and non-roughness model from general modelling 38

Figure 5-4 Dispersion curve from general and corresponding Cauchy model 40

Figure 5-5 Refractive index vs. deposition rate 42

Figure 5-6 Surface roughness vs. deposition rate 44

Figure 5-7 Possible trends of refractive index with deposition rate 45

Figure 5-8 Dispersion curves from general model and corresponding Cauchy model at 0.1, 1.6, and 3.0 Å/s deposition rate 46

Figure 5-9 Refractive index of Al metal and alumina within 300-1200nm wavelength rage 47

Figure 5-10 Variation of refractive index and surface roughness with additional oxygen in the chamber 48

Figure 5-11 Dispersion curve change after exposure to air at room temperature for more than 24 hrs 49

Figure 5-12 Refractive index increase upon exposure to air for samples deposited with additional oxygen in the chamber 50

LIST OF SYMBOLS AND ABBREVIATIONS

Ebeam	Electron Beam
VASE	Variable Angle Spectroscopic Ellipsometry
Al_2O_3	Aluminum Oxide, Alumina, or Sapphire
LED	Light Emitting Diode
MIM	Metal-Insulator-Metal
PVD	Physics Vapor Deposition
CVD	Chemical Vapor Deposition
ALD	Atomic Layer Deposition
DC	Direct Current
RI	Refractive Index
IBAD	Ion Beam Assisted Deposition
XPS	X-ray Photoelectron Spectroscopy
XRD	X-ray Diffraction
AES	Auger Electron Spectroscopy
P	Pressure
R.F.	Radio Frequency
Å	Angstrom

Symbol	Meaning
K.E	Kinetic Energy
eV	Electron Volt
B	Magnetic Field
h	Plank’s Constant
ν	Frequency
c	Velocity of Light
λ	Wavelength
k_B	The Boltzmann Constant
H_2SO_4	Sulphuric Acid
H_2O_2	Hydrogen Peroxide
N_2	Nitrogen Gas
T	Temperature
Z	Acoustic Impedance
k	Extinction Coefficient
MSE	Mean Square Error
Al	Aluminum
Si	Silicon
O or O_2	Oxygen atom or molecule

1. INTRODUCTION

1.1 Background

Thin films are used in many industries, and are of particular importance in the semiconductor device industry. Electron beam (ebeam) deposition is used in device fabrication. The goal of this research project was to investigate the deposition and characterization of aluminum oxide films deposited by electron beam evaporation. For films characterization, a Variable Angle Spectroscopic Ellipsometry (VASE) tool was used.

Aluminum oxide or alumina (Al_2O_3) is a refractory ceramic oxide that is widely used in many industries. It is found in nature as corundum or α-Al_2O_3 that has a hexagonal crystal structure with closed packing aluminum and oxygen atoms. This closed packing structure leads to good mechanical and thermal properties. It has a high free energy of formation of -1582.4 $kJ.mol^{-1}$ [1] which makes it chemically stable and refractory material. It has melting point of 2072°C. These qualities make alumina desirable for make applications such as wear and corrosion resistance, biomedical, metal cutting tools, milling media, and many more. Single crystal aluminum oxide (sapphire) is one of the hardest natural minerals, second only to diamond. It has a stable dielectric constant, very low dielectric loss, good electrical insulation and thermal conductivity, high heat resistance, low ionic mobility of impurities, and higher breakdown voltage.

Alumina has been in industrial use for many applications due to these properties. It is used as a protective layer because of exceptional hardness and adhesion. Sapphire is also used as substrate for blue LEDs.

In this research silicon (100) substrates were used for deposition experiments. Aluminum oxide thin films were deposited by ebeam evaporation and characterized by VASE ellipsometer. It was found that film quality changes with deposition rate or electron beam current.

1.2 Organization of Thesis

Thin film depositions of alumina by ebeam evaporation are reviewed in the literature review in chapter 2. The deposition system and control parameters are described in chapter 3. Chapter 4 includes the experimental procedure in which thin film deposition and control parameter procedure and the characterization techniques are described. Results and discussions are detailed in chapter 5 followed by conclusions and future work in chapter 6.

2. LITERATURE REVIEW

Higher dielectric constant materials are needed for future generations of devices including logic and memory devices to reduce leakage current as device sizes are getting smaller. Alumina has dielectric constant of 11 and a refractive index (RI) of 1.766 at wavelength 630 nm [2]. Aluminum oxide has many desirable qualities and is a possible candidate in replacing SiO_2 as a gate oxide. It is a possible candidate for Metal-Insulator-Metal (MIM) tunnelling diodes. The ability to grown sub 100 nm thick films and quality of the film are two of the most important factors for tunnelling devices.

2.1 Thin Film Aluminum Oxide

Aluminum oxide thin films have been deposited by sputtering, CVD, ALD, ebeam, and by anodic and native oxidation. Sputtering and ebeam deposition systems have been modified to increase film quality by adding substrate rotation, substrate heating, ion-beam bombardment, substrate heaters, and beam chopping instruments. The properties of thin films are often different than bulk properties. Density, crystal structure, and stoichiometry of the film change from that of bulk material. The change in quality of the film affects electrical and optical properties such as dielectric constant and refractive index of the film.

Many different phases of Al_2O_3 have been observed. However α-Al_2O_3 and γ-Al_2O_3 are well known stable and metastable phases, respectively. At lower substrate temperatures, the Al_2O_3 films are amorphous when grown by ebeam reactive deposition. In order to get crystallization in ebeam Al_2O_3 films, a post deposition annealing and/or substrate heating are required. As the substrate temperature gets higher, film density and crystal structure change. Aluminum oxide transforms to crystalline γ- and α-Al_2O_3 phase at 300-900°C and above 650-1000°C [5], respectively. Mechanical, electrical and optical properties of the film change with deposition condition and film structure. Different phase structures of Al_2O_3 correspond to different binding energy. Metastable γ-Al_2O_3 has ionic bonding which has less binding energy than stable α-Al_2O_3 which has covalent bonding with higher binding energy. When ion assisted reactive evaporation was done, γ-Al_2O_3 was achieved at substrate temperature less than 250°C. This occurred because the Al_2O_3 phase structure changes with oxygen ion energy and transport ratio [7]. Crystallization enhances the hardness of the film. In reactive Al evaporation, the hardness of Al_2O_3 films tend to decrease with increasing Al/O composition ratio due to the formation of the metallic films [5].

2.2 Aluminum Oxide Deposition by Electron Beam Evaporation

Alumina (Al_2O_3) films have been deposited by e-beam evaporation using two methods:

- From source Al metal and oxygen gas in reactive evaporation.
- From source alumina with or without additional oxygen in the chamber.

Oxygen ion beam bombardment on the substrate, known as ion beam assisted deposition (IBAD), can be used during deposition process with Al or alumina sources. A chopping tool can also be used during deposition in ebeam evaporation to study the kinetics of film growth.

2.2.1 Aluminum Oxide from Source Al with Oxygen Gas

In reactive alumina deposition, Al metal vapour reacts with oxygen gas to form alumina compound [8]. The overall chemical reaction for this process is shown below.

$$2\ Al\ (vapour) + 3/2\ O_2\ (gas) \leftrightarrow Al_2O_3\ (solid\ deposit)$$

Incomplete aluminum oxidation allows the formation of suboxide compounds which could achieve full stoichiometry in the presence of oxygen in the chamber. The reaction between metal vapour and reactive gas molecules take place on substrate, in vapour phase, and at the source surface. Oxidized target molecules

may dissociate immediately because of continuous heat supply. However, if the oxygen pressure is high, target oxidation would dominate and reduce the deposition rate significantly.

A collision between reactant species does not necessarily ensure that reaction will occur. Reaction yield or probability of reaction between species have been shown to be enhanced by activating one of the reactants by, for example, ionizing oxygen during reactive deposition with Al vapour source [8]. In ion beam assisted deposition, a reactive gas ion source created ions that accelerate toward the substrate. Refractive index and electrical properties were significantly enhanced with crystallization of the film. Ion beam assisted films have been shown to have the ability to work as optical waveguides [10]. However, an amorphous alumina film works well as an insulator [4].

Bunshah et al [8] reported activated reactive deposition technique for compound films from metal and reactive gas in ebeam evaporation to get the high deposition rate. In activated reactive deposition, metal from high rate evaporation source react with oxygen gas in the vapor phase to form deposit alumina. A positively biased 80-200V dc probe was used to draw some electrons from above the molten target pool into the vapor phase reaction zone which was between the substrate and the source. These electrons activated the metal vapor and oxygen gas to increase reaction yield. The compound formed in vapor phase then deposited on

the substrate. In this process, compound formation and deposit growth can be controlled separately which is a major advantage in controlling film properties.

The electrical properties of the alumina films grown from source Al with oxygen gas by ebeam evaporation were characterized by DaSilva et al [9]. They found that the dielectric constant of the films changes upon exposure to air. They assumed that changes in dielectric properties of the films were due to formation of stoichiometric films from suboxide components upon exposure to air. Both oxygen and aluminum supply need to be controlled in order to get the desired film quality and stoichiometry. Low oxygen pressure gave metallic films with low resistance. As aluminum evaporation rate was decreased and oxygen pressure was increased, resistivity of the film increases to exhibit insulating behaviour. Films' appearance changed from metallic to transparent form as oxygen supply was increased.

Yoon et al [11] deposited aluminum oxide using the activated reactive ebeam evaporation technique. Films were deposited from source Al with oxygen plasma. They used a high power electron beam source and high oxygen flow rates to get a deposition rate as high at 8μm/hr (2.22 nm/sec). A substrate temperature of $300^{o}C$ was used. A very close relation between the electron beam current and the oxygen pressure was observed. As oxygen pressure increased, the Al molten pool area decreased reducing the deposition rate. It was also observed that the refractive

index and the density of the film depended on the Al/O flux ratio. They concluded that higher values of RI in alumina films occurred due to the aluminum-rich films.

Nightingale et al [10] used oxygen ion beam assisted ebeam (IBAD) evaporation with source Al to form high quality alumina films. It was observed that use of ion source bombardment with an alumina source enhanced the control of refractive index and optical losses. Alumina films deposited with oxygen ion bombardment were found to work as waveguides. Alumina source material with 99.99% purity and of 2-12 mm with grain size was used for these experiments. Refractive index was found to be dependent on ion source control parameters such as oxygen gas flow rate and ion source drive current. Refractive index was found to be within the range of 1.58 to 1.64 measured by ellipsometer at 633nm wavelength. It was observed that refractive index decreases with increasd oxygen pressure. Alumina films deposited without ion beam assistance has RI of 1.6173 at 633 nm wavelength. It was also observed that non-IBAD alumina films of RI 1.6137 at 633 nm were unable to guide light. However, IBAD films with lower indices made good waveguides. It was reported that the higher refractive index of non-IBAD films were due to water filling the void columns of the low density films. They observed that increasing oxygen flow lowers both mean ion energy, ion current density, and drive voltage resulting in film density and RI decrease with increasing oxygen flow.

Shimizu et al [5] deposited alumina films from source Al and oxygen ion beam in ebeam evaporation. They subjected substrates to bombardment with oxygen ions of energy 2-24 keV with an Al/O flux ratio from 0.5 -14. Films were characterized by X-ray photoelectron spectroscopy (XPS) for elemental composition and X-ray diffraction (XRD) for crystal structure. Films deposited with oxygen ion energy of 20-23 keV and Al/O ration of ~ 0.67 showed the crystal structure of γ-Al_2O_3. Films were deposited on Si (100) wafers and glass substrates. The refractive index of the samples exhibited the γ-Al_2O_3 structure was found to be 1.62 at 633 nm wavelength. In reactive alumina deposition from vapour Al and working oxygen gas, the Al/O transport ratio was found to be a very important factor in determining the stoichiometry of the films. The transport ratio is defined as the ratio of the vapour aluminum atom flux (atoms/ (cm^2.s)) to the oxygen molecule or ions (molecules (or ions)/(cm^2 s)). The Al/O composition ratio of the films was characterized by XPS. They also found that hardness of the films decreased with increasing Al/O ratio due to the formation of metallic films.

2.2.2 Aluminum Oxide from Source Alumina

Aluminum oxide films have also been deposited by direct evaporation of source alumina. Ebeam deposition has been used to achieve the high temperatures required for the evaporation of refractory materials. Refractory materials often dissociate during evaporation depending on melt temperature. Dissociated suboxides are unstable and susceptible to contamination [9].

Stoichiometry of the refractory films have been controlled by using the equilibrium condition of the chamber vapour pressure and temperature [12]. At higher temperatures, incomplete alumina film stoichiometry has been improved by adding oxygen in the chamber. Al, O, AlO, Al_2O etc. atoms and compounds have been shown to form after dissociation during aluminum oxide evaporation. At a given temperature, alumina vapour pressure needed to be at higher than the equilibrium value of the dissociation pressure in order for stoichiometric alumina deposition to occur. However, the low temperature dissociation of alumina may be caused by the interaction of alumina molecules with crucible material. Film stoichiometry was improved by adding oxygen in the chamber.

Eriksson et al [3] deposited and characterized alumina films deposited by ebeam evaporation from source alumina pellets of purity 99.992%. A high power electron beam source of 8 kW was used. The evaporation rate was 0.7 nm/s with a source to substrate distance of 55 cm with a deposition pressure of 2 $x10^{-5}$ Torr. Films thickness varied from 0.3 to 3.6 μm. Refractive index was measured by spectrophotometric recording within the wavelength of 350 nm to 2100 nm range that gave RI of 1.61 at 630 nm. They have compared their results to other published work, as shown in Figure 2-1.

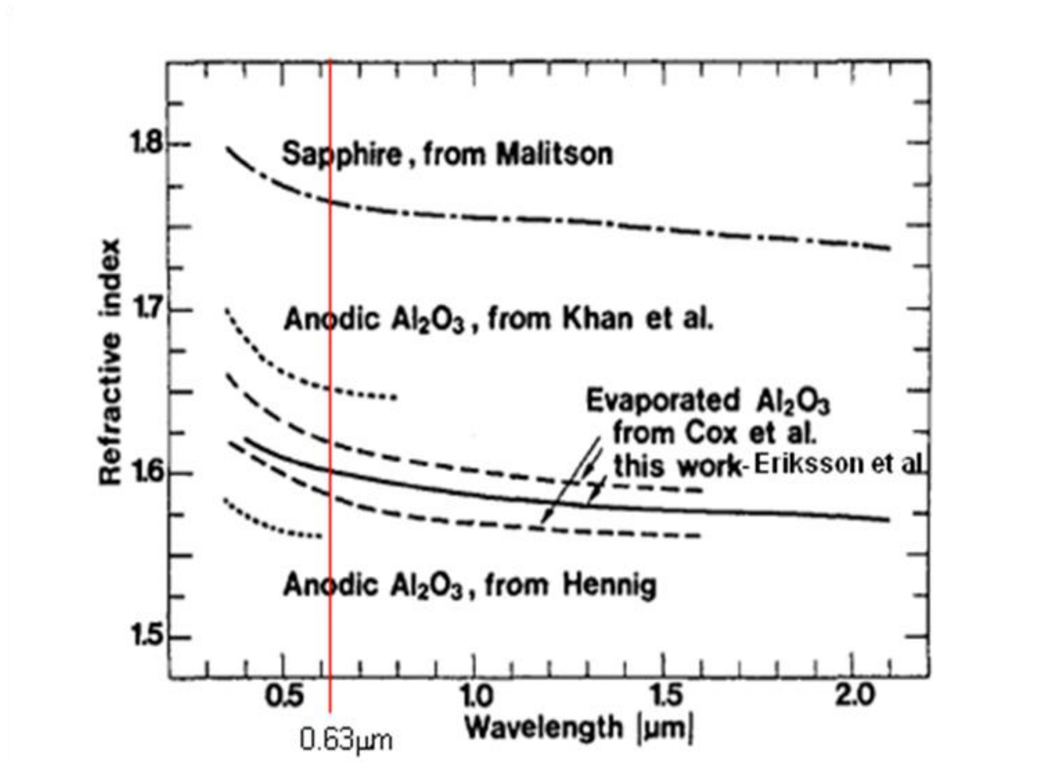

Figure 2-1 Alumina dispersion curve comparison deposited by different deposition techniques [3]

Cox et al [16] have deposited alumina from source alumina at 40°C and 300°C substrate temperature by ebeam evaporation. They observed that high substrate temperatures increase refractive index. The refractive index increased from 1.6 to 1.63 with an increase in the temperature from 40 to 300°C at 500 nm wavelength.

Hoffman et al [17] have evaporated alumina on to silicon substrates from an alumina source in dry and wet oxygen ambients. Ellipsometry was used to

characterize refractive index. It was noticed that growth and uniformity of the films depended on the type of substrate used, the evaporation rate, the substrate temperature, and the chamber atmosphere. They characterized the variation of refractive index with films thickness by etching grown films in stepwise fashion. It was noticed that the etch rate was lower for the top layer of the as deposited films. They concluded that the top layer of the films continued reacting with surrounding oxygen during cool down after deposition. Films deposited in dry oxygen were more homogeneous and denser than films prepared in wet oxygen atmosphere. Dry oxygen deposited films had a slow etch rate. Refractive index variation with thickness for dry oxygen ambient films was small compared to films deposited in wet oxygen ambient. Refractive index of dry oxygen ambient films did not change significantly within the range of 40 to 100 nm thickness.

Matolin et al [12] ebeam evaporated thin alumina films from an alumina powder source of 40 μm grain size and purity of 99.999%. The stoichiometry of the films was monitored by in situ Auger Electron Spectroscopy (AES). Deposition was controlled with a very low power ebeam source that gave a very low deposition rate. AES analysis showed that the stoichiometry of the films depended on the evaporation rate that corresponded to the ebeam emission power. It was shown that stoichiometric films could be deposited with electron emission powers of up to 12 W that gave a source temperature up to 1777 ^{o}C (lower than the alumina melting point). The deposition rate was 3 nm/hr with a source to substrate

distance of 5 cm. According to their calculations, growth of stoichiometric alumina films should be possible at temperatures up to 2727 ^{o}C. However, films deposited at temperatures between 1777 and 2727 ^{o}C were aluminum rich when deposited at higher evaporation rates with 12-15 W beam power. At beam powers greater than 15W, films were metallic.

Kubler et al [13] deposited alumina films from source alumina with and without ion beam assistance in an ebeam evaporation system. They found that films deposited with oxygen ion bombardment have better dielectric properties than that of the films deposited without ions bombardment but otherwise identical deposition parameters. Oxygen ions were generated by an r.f. source and accelerated to the substrate with energies from 0-200 eV. The effect of ion bombardment on the dielectric properties of the films were compared with films deposited without ion bombardment. Non-IBAD films were reactively deposited from oxygen gas and an alumina source at a deposition rate of 0.1-1.2 nm/s. Ion beam assisted deposition increased the density of the films which improved the optical and electrical properties of the films. A gravimetric density measurement was used to measure the density of the films. Non-IBAD films had density of 3.0 gm/cm^3 ± 5% and IBAD films had density of 3.6 gm/cm^3 ± 5%. Non-IBAD films exhibited an inhomogeneous porous structure that was not found in IBAD films when characterized by transmission electron microscopy. Alumina films deposited without ion assistance exhibited a porous structure with incomplete bonding. The inhomogeneities in the porous films gave different electrical

properties in different regions of the films. It was observed that evaporation rate also influenced the homogeneity of the films and that affected the film electrical properties. Films deposited by IBAD had higher resistivity and better dielectric properties than non-IBAD films.

A novel two step process was developed by Saraie et al [14] to get high quality alumina films by ebeam evaporation from source alumina with oxygen in the chamber. A very thin, 10 nm thick, alumina layer was deposited at room temperature and a second layer was deposited at 250 ^{o}C on top of the first layer, without breaking vacuum. Films deposited with the two step process had high breakdown field and small leakage current at high electric field. Samples were also deposited by a one step process at room temperature and at 250 ^{o}C. Films at room temperature were deposited at a rate of 0.4-3.0 Å/s and it was shown that the resistivity and the breakdown field increased with decreasing the deposition rate from 2 to 0.4 Å/s. Oxygen supply increased resistivity but decreased the breakdown field. On the other hand, the resistivity of the films deposited at 250°C were high and only varied slightly with the deposition rate. In the one step process, films deposited at 250 ^{o}C were considered to be inhomogeneous and consisted of a well developed polycrystalline structure with grains and grain boundary regions. The initial layer had an island-like structure due to reduction of nuclei density with decreased mobility of the ad atoms on the surface. The initial island-like structures influence the ad atoms that are deposited on top of it. The high temperature one step deposition gave high resistivity. However, in the one

step process, high temperature films had lower breakdown fields than that of films deposited at room temperature. In the two step process, the first room temperature layer covers substrate uniformly. This initial uniform alumina layer works as a good nucleation site for the following high temperature ad atoms and give a homogeneously well structured film.

Patil et al [15] used a chopper inside ebeam evaporation system during alumina deposition from source alumina to chop the alumina flux. It was found that alumina films deposited in this manner give higher refractive index and better adhesion than that of films deposited without chopping. Chopping helped to create closely packed structure and to increase adhesion of the films.

3. ELECTRON BEAM DEPOSITION SYSTEM AND CONTROL PARAMETERS

Ebeam evaporation is a pvd technique that utilizes the phase change of a material from the condensed to the vapour phase. Ebeam deposition technology was invented by Charles W. Hanks in 1960 [18].

3.1 Electron Beam Evaporation System

All evaporation techniques require thermal energy supplied by heating either by resistive heating or ebeam heating. In resistive heating the source is melted by a heated wire. For very high temperatures electron beam evaporation is used. A schematic diagram of a typical electron beam evaporation system is shown in Figure 3-1. In this system, a magnetic field is applied perpendicular to the direction of propagation of the electron beam and is used to bend and shape the electron beam. It is necessary to protect the ebeam source from vapors that evolve during evaporation process. This is done by placing the electron source (filament) below the crucible and out of sight of the evaporant atoms [18]. As electrons are focussed and strike only source material, contamination from the crucible is non existent.

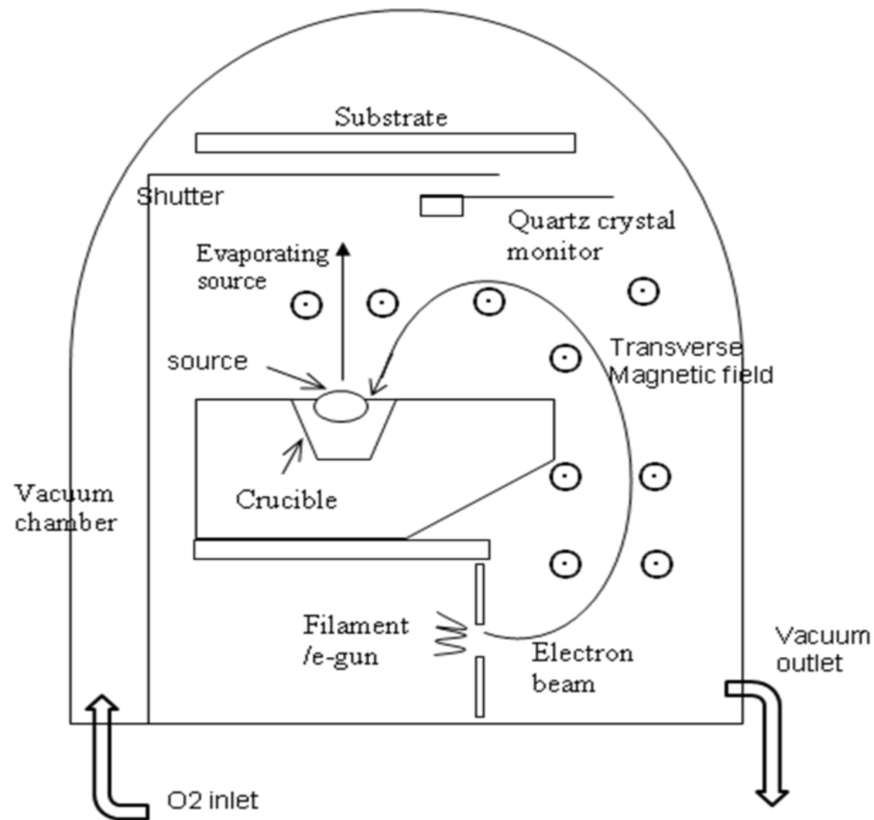

Figure 3-1 Schematic diagram of electron beam evaporation system

3.2 Control Parameters

Ebeam evaporation has two categories of control parameters, power supply and chamber parameters. The power supply control parameters of interest are acceleration voltage, supply current, power density, diameter of the electron beam, and beam sweep area. Chamber parameters are chamber pressure, gas type, source to substrate distance, substrate rotation, substrate temperature, crucible

design, and water cooling. Both power supply and chamber parameters affect the interaction between the electron beam, gas molecules, and target materials, as well as the melting temperature and the deposition rate. In the following sections, some of these parameters will be discussed in more detail.

3.2.1 Acceleration Voltage

The target (source) material is kept as anode that accelerate electron beam. The target anode directs and accelerates the electron beam. The electron kinetic energy is defined by K.E = eV in an electric field potential V that usually ranges from 10-40 kV in an ebeam system. Velocity of the electrons increases with the electric field potential. Electron kinetic energy is converted into many forms of energy after interacting with the target. When the electron beam hits the target, a number of interactions occur between the incident electrons and the target material. Some electrons reflect back and are called backscattered electrons. Secondary electrons are electrons that are decelerated by collisions and re-emerge from the surface of the evaporating target. Most of the kinetic energy of the beam converts into heat. New electrons can also be generated from the target surface by thermionic emission. As electrons decelerate, they also emit electromagnetic radiation over a range of wavelengths where the minimum wavelength or maximum frequency is given by

$$eVB = h\nu_{max} = hc/\lambda_{min}$$

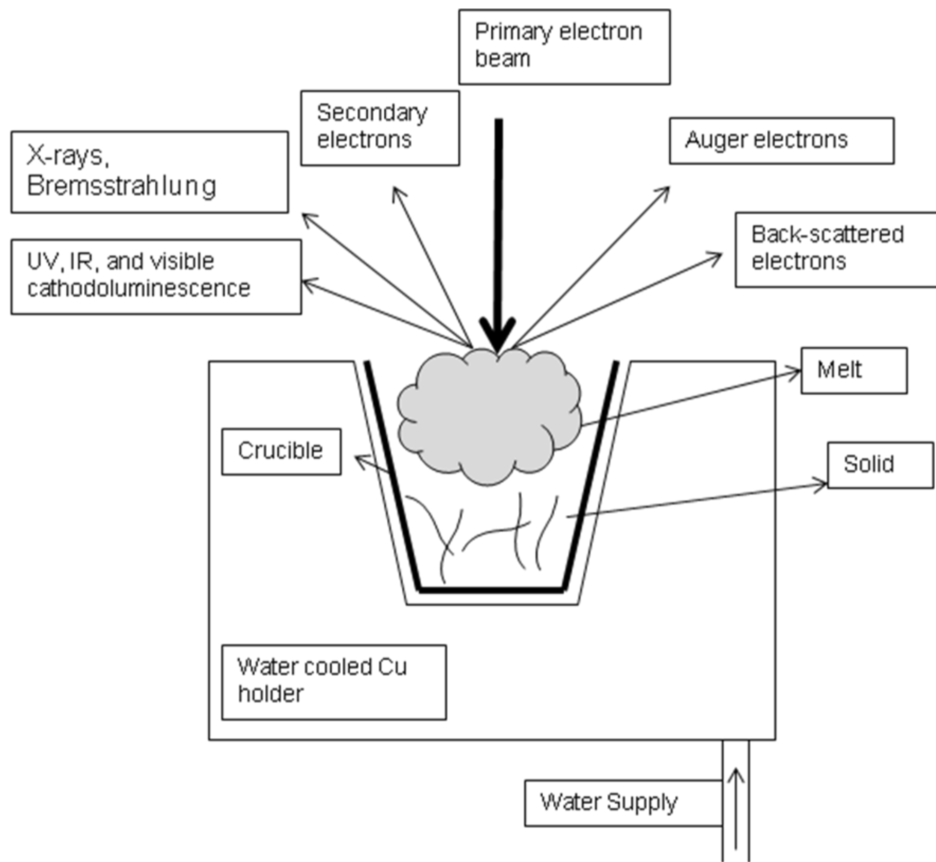

Figure 3-2 Electron beam interactions with target

For the higher voltage, the wavelength corresponds to the x-ray wavelength. A range of continuous wavelength, from λ_{min} to λ_{max} with maximum intensity around λ_{min}, may generate continuous radiation known as bremsstrahlung radiation. Electrons also ionize some of the evaporating atoms that radiate electromagnetic wave when the ions relax to the ground state. The wavelengths of the corresponding radiation are characteristic of the energy levels of the excited atoms [19].

3.2.2 Beam Current

One of the control parameters for the system is electron beam current. Higher beam current gives higher energy density on target. Atoms leaving the surface of evaporant material have average energy of ($3/2k_BT$), where k_B is the Boltzmann constant [19]. Higher energy density gives more heat and hence more energy to the evaporant species. Deposition rate depends on supplied heat. As heat increases, more target material evaporates. Beam current is one of the main control parameters in the ebeam system.

3.2.3 Sweep Area

Beam sweep area is related to power density. Electron beam rastering is important in order to obtain thermal stability over the target area. Larger sweep areas give better control of deposition rate. Rastering reduces evaporant spikes and dips due to unstable melting points, and decreases deposition rate fluctuation. Extreme high power density focussed to a point causes splashes in molten liquid. It is very important that the source material is pure. A macro impurity particle with different vapour pressure can suddenly be ejected from the surface causing rate fluctuation and hillocks and holes in the films. Larger sweep area gives lower power density that reduces deposition rate. Rastering reduces the energy of the species leading to a lower density film.

3.2.4 Source to Substrate Distance

Deposition rate and film quality depend on the substrate to source distance. The velocity of the species leaving the source follow the Maxwellian distribution of velocities. Evaporant material flux is directional and follows the cosine emission law in which mass flux of evaporant molecules at a distance r from the source is a direct function of $\left(\frac{\cos\theta}{r^2}\right)$, where θ is the angle between the normal to the substrate and the direction in space of the evaporating flux from r distance. Therefore a shorter source to substrate distance will give higher deposition rate. The energy of the atoms evaporated from the melt is of the order of 0.1- 0.2 eV which is about one to two times the average thermal energy 3/2 k_BT expected from the source material temperature. This higher energy is due to the electrons exciting atoms to higher energy states and subsequent conversion of potential energy into kinetic energy as the atoms move away from the evaporation source [19]. A shorter substrate distance gets heat directly from the source and captures highly energetic species that, due to energy conversion, will increase substrate temperature. Depending on the particular film material, a shorter distance should also give more densely packed films. A fixed source to substrate distance was used in our experiments.

3.2.5 Substrate Temperature

Substrate temperature is an important deposition variable. Higher substrate temperatures increase film density due to increased mobility of the deposited species. However, higher temperatures may cause thermal stresses in the films due to thermal expansion coefficient mismatch between the film and the substrate. No substrate heating was used in our experiments.

3.2.6 Chamber Pressure

Mean free path of evaporated species are inversely proportional to the pressure of the chamber or the partial pressure of the reactant species in the chamber. If the mean free path is longer than substrate to source distance, no collisions will occur between reactant species in the vapour phase. These reactions will occur at the substrate surface. Therefore low partial pressure implies a low source temperature resulting in a low deposition rate. A greater supply and hence higher partial pressure and smaller mean free path of reaction species are needed for higher deposition rate. Smaller mean free path leads species to collide in the vapour phase and on the substrate. The vapour phase collisions form compounds which later deposit on the substrate and increase deposition rate [8].

As chamber pressure decreases, evaporant species collide less with each other and gas molecules. Low chamber pressure evaporant species have longer mean free path and lose less energy in collisions. A higher density film is possible because

of increased mobility of the deposited species. Electron beams lose energy in inelastic collisions with gas atoms by ionizing or exciting atoms. If evaporant atoms have sufficient energy, it increases film quality by improving microstructure with densely packed atoms. Ebeam deposited films typically have columnar microstructure, with low density voided regions due to the low surface mobility of evaporated atoms and molecules [10]. In summary, deposition rate and film quality also depend on the mean free path and substrate to source distance. High chamber pressure also affects the electron source filament lifetime by erosion and arching. Arching happens due to potential difference between filament and nearby gas components.

3.2.7 Crucible and Water Cooling

A good crucible and pocket design increases proper energy utilization [19]. Due to localized direct heating the electron beam source is used to deposit low and high melting point materials that include highly reactive and refractory materials. A water cooled copper pocket is used to cool the crucible. A crucible with better cooling allows evaporation of high melting point materials. A good cooling crucible is possible when the crucible is in good contact with the evaporant and the cooled copper pocket. Heat transfer causes heat loss that causes lower target temperatures. In this case a higher power beam source is required for higher heating. On the other hand, if heat transfer is not enough, the crucible material starts reacting with source materials or causes higher temperatures than expected.

An insulating material can be used to reduce heat transfer and act as a barrier that subsequently reduces higher power use and increases target temperatures.

In our experiments, all parameters were fixed except for electron beam current and sweep area. The system did not have any substrate rotation or heating capability. Substrate rotation would increase uniformity and homogeneity in the films. Source to substrate distance were fixed to 40 cm and acceleration voltage were fixed to 6.0 KV. Therefore the main concern of our research was to understand film quality variation based on beam current variation. Sweep area was kept as small as possible while maintaining a stable deposition rate.

4. EXPERIMENTAL PROCEDURE

4.1 Sample Preparation

Silicon (100) substrates were used for deposition experiments. 100 mm diameter Si (100) wafers were cut into 1 by 0.5 inch pieces using a wafer dicing saw. The dicing saw, Disco DAD 321, is an automatic, programmable system. The saw can cut rectangular, irregular, and circular shape pieces. Prior to cutting the wafer adhesive was placed on the back of the wafer. The wafer was cut into rectangular samples wherever possible. After cutting the wafer into small pieces, the pieces were kept in a large wafer holder with the dicing tape attached. The small wafer pieces were separated from the tape prior to cleaning. Wafer holders were cleaned with acetone followed by air-gun dry.

4.1.1 Wafer Cleaning

Silicon wafers are usually not clean and the surface contains many small dust particles, organic molecules, skin oil, lubricants, inorganic salts, ions, metal atoms, and native oxide. Device yield depends on the cleanliness of the silicon substrate and equipments. In order to reduce contamination, industry uses automated equipments and very high level clean room facilities. For our experiments processing was done manually and in the 10k clean-level area of the Nanofab in Electrical Engineering.

Standard piranha solution was used for the wafer cleaning in a class-100 clean area. The piranha solution is made with a mixture of sulphuric acid H_2SO_4 (96%) and hydrogen peroxide H_2O_2 (30%) solution at volume ratio of 3:1. The piranha solution removes most dust, organic and inorganic contaminants. However it does not remove native oxide. Since native oxide did not affect our experiments it was not removed from wafer. Both H_2SO_4 and H_2O_2 are dangerous chemicals and a special wet station facility reserved for piranha cleaning was used. The wet station is equipped with ventilation, chemical drain, and water aspirator. Prior to the cleaning, chemical apron, gloves, and helmet were worn. Separate containers were marked for respective amounts of H_2SO_4 and H_2O_2 and were filled with the respective chemicals. H_2SO_4 was poured first into the bigger mixing container followed by adding the H_2O_2 in small amounts increments. Upon contact, both chemicals react and the solution temperature rises to 100^oC. The teflon carrier bucket, with widely spread wafer pieces, was put into the piranha mixture for 15 minutes. After 15 min, the bucket was taken out carefully and put into a water rinsing station. The bucket with the wafer pieces was rinsed 5 times to make sure that no chemical was left on the wafers. The wafer pieces were dried individually with an air gun. Small, previously cleaned, wafer holders were used to store the individual wafer pieces and were put in a clean container.

4.1.2 Native Oxide Thickness Measurement

Silicon wafers readily grow a native oxide when exposed to air. Native silicon oxide needs to be considered prior to any experiment since alumina dielectric would be deposited on silicon wafers with native silicon oxide. The thickness of the native oxide was measured by ellipsometer and found to be 2 to 2.6 nm thickness. For measurement of the optical properties in a multilayer structure, 2 nm is at the lower limit of thickness measurement for the VASE ellipsometer. Therefore, native oxide was not included as separate optical layer in VASE modeling. Instead, the native oxide layer was incorporated with the thickness of deposited Al_2O_3 as the same material layer.

4.2 Film Deposition

Electron beam evaporation was used to deposit alumina thin films. The system that was used is located in the Nanofab in Electricial Engineering. The vacuum chamber and system was made by Kurt J. Lesker and it had a cylindrical metal bell jar shape. The system has manual operations and analog power supply as shown in Figure 4-1. The power supply was Airco Temescal, model ES 6. The chamber was pumped down with a mechanical and a cryogenic pump. Chamber pump-out and oxygen supply control was manual. Chamber pressure reading was an analog meter reading and oxygen supply reading was manual rotating meter reading.

Figure 4-1 Electron beam deposition system used in the project

A quartz crystal thickness monitoring system was used to monitor film thickness in situ during deposition. The piezoelectric sensor that measures the thickness in the system was checked prior to every deposition and was replaced if life time was less than 80%. In almost all experiments, the piezoelectric sensor had more than 90% life span available. Crystal monitoring system needs to be set by setting 3 parameter values needed for individual target materials. They are density, z value, and tooling factor. Density is the target material density and was 3.96

gm/cm^3 for alumina. Z is the acoustic impedance of the deposited material defined by the ratio of sound pressure to the velocity in a medium. Z-value is more important for thicker films [20]. The z-value for aluminum oxide is not specified. However a specific value of 0.36 was used. The tooling factor is defined as the ratio of deposited film thickness on the sample to the film thickness on the sensor. A tooling factor of 100% was used that gave almost same thickness measured by both crystal monitoring and ellipsometer due to the small substrate to sensor distance. Changing tooling to 110% gave more thickness than the ellipsometer measurement.

Alumina films were deposited from source alumina. Small grains of target alumina particles as shown in Figure 4-2 with a size of 1.5 to 4 mm were put in a coated graphite crucible that was placed in a copper water cooled anode. Two sets of films were deposited, one set with oxygen and another set without oxygen in the chamber.The purity of the target material was 99.99 wt% with impurities of $<0.0001\%$ Cd, $< 0.0001\%$ Cr, 0.004% Na, and $< 0.0002\%$ Pd [21]. Oxygen purity was 99.99%.

Figure 4-2 Used alumina source grains in coated graphite crucible

A cleaned Si substrate was mounted straight 40 cm above the target. A shutter was located in between the substrate and the source. This prevented deposition on the substrate while the electron beam was being set up and the source was coming to temperature. The shutter was movable from outside the chamber without breaking vacuum.

After putting the substrate and target material in the system the chamber was evacuated using the roughing pump until the pressure was about 300 mTorr. At this pressure, the roughing pump valve was closed and the cryo pump valve was opened. It took around 2 hours to reach the expected base pressure in the

chamber. About 90 minutes into the pump down, the electron beam source was turned on with low power for approximately half an hour to outgas and pre clean the target surface. After outgassing and before deposition, the beam power was turned off and the base pressure was recorded. For deposition the electron beam was turned on and the chamber pressure increased due to the vapour pressure of the source. When higher beam current was used for deposition, outgassing was done for a longer time in order to reach the expected deposition pressure.

After recording the base pressure, beam current was turned on again and optimization of the beam current, sweep area, and deposition rate was initiated. In order to obtain a constant deposition rate, the beam sweep area was kept larger initially to permit a bigger melting area and good target heat stability. After few minutes, the sweep area and beam current were decreased until the expected deposition rate was obtained. The specific deposition condition was monitored for few minutes to make sure there was no fluctuation. At this point the deposition pressure was recorded.

For samples deposited without oxygen supplied to the chamber, once stable deposition rate was set, after recording base and deposition pressure, thickness monitoring system was reset to start reading and shutter was moved out of the way of substrate. During deposition, if the rate fluctuated, the sweep area was changed and the beam current was kept constant. Changing beam current was very sensitive and could make the fluctuations worse. Increasing sweep area

without changing other parameters decreases deposition rate. Several samples were prepared by varying the deposition rate from 0.1 to 3.0 Å/s.

For samples deposited with oxygen in the chamber, the flow of oxygen ranged from 0.5 to 4.0 sccm. Oxygen supply was turned on after measuring base pressure and few minutes before deposition started. With the oxygen flow on, more beam current was needed as deposition rate goes down dramatically with the higher chamber pressure. Deposition rate for samples deposited with oxygen was fixed at 0.2 Å/s. When deposition was finished, the oxygen flowed for few minutes after turning off the beam power.

Once the required film thickness was reached, the shutter was immediately closed to block the incoming species impinging on the wafer and then the beam power was turned off. The chamber was kept under vacuum for at least 15 minutes to let the source cool down. After 15 minutes, the cryo pump valve was closed, the ionization gauge was turned off and the N_2 gas valve was opened to vent the chamber to atmospheric pressure.

Prior to the next deposition, the top molten and surrounding discoloured alumina particles in the source were thrown away. New alumina grains were used as a top layer in the crucible prior to every deposition. The time between from deposition to VASE measurement was approximately 25 minutes. Deposition parameters are summarized in table below for samples deposited both with and without oxygen.

Table 4-1 Deposition Parameters

Parameters	With oxygen	Without oxygen
Deposition pressure, Torr	$1\cdot10^{-5}$ to $5.3\cdot10^{-5}$	$1\cdot10^{-6}$ to $2\cdot10^{-6}$
Base pressure, Torr	$6\cdot10^{-7}$	$4\cdot10^{-7}$ to $8.5\cdot10^{-7}$
Deposition rate, Å/s	0.2	0.1 to 3.0
Beam source current, mA	22 to 30	20 to 45
Thickness, nm	38 to 43	28 to 41

4.3 Film Characterization

A Variable Angle Spectroscopic Ellipsometry (VASE) was used for film characterization. VASE is a non-destructive, accurate, and versatile material characterization tool that has been used to characterize semiconductors, dielectrics, polymers, metals, and many other materials [22]. It measures thickness in nm level and optical constants for sample with thicknesses greater than 10 nm. A schematic diagram of a VASE optical set up is shown in Figure 4-3 . In the VASE a polarized beam of light, either linear or circular, is directed at the sample and the reflected or transmitted polarization condition of the beam is measured by a detector. The known phase of parallel and perpendicular components of the beam changes upon interaction with sample electrons.

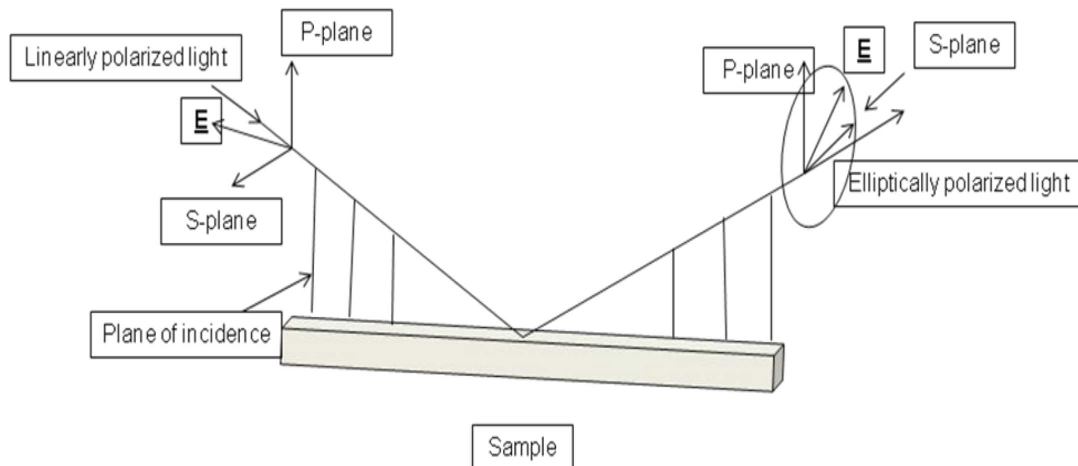

Figure 4-3 Schematic diagram of ellipsometry working process

This change in phase causes a polarization change and is measured by the detector. Optical constant and thickness can be determined by a fixed angle ellipsometry. The use of variable angle ellipsometry only increases the sensitivity of the measurements [23]. The system used in these experiments was a HS-190, made by J. A. Woollam Company, with spectral range 300-1700 nm. The computer software version was WVASE- 32. The system has a rotating optical sensor to measure the variation of the intensity of the light with corresponding change in polarization upon reflection off the sample surface. A picture of the VASE is shown in Figure 4-4

©J.A. Woollam Co., Inc.

Figure 4-4 VASE system used from J. A. Woollom Co., Inc.

In order to measure the optical constants of a dielectric material, minimum sample thickness of ~10 nm is required [23]. With thickness less than 10 nm, the sample is not thick enough to cause much change in the orientation of the electric field vectors with the change in phase between parallel and perpendicular components of the field. With thickness higher that 10 nm, this change is more significant and this increases measurement sensitivity. For thickness less than ~10 nm, only thickness can be measured if RI is known. But for thickness greater than 10 nm, both optical constants and thickness can be measured simultaneously.

5. RESULTS AND DISCUSSIONS

5.1 Optical Characterization

Samples were characterized immediately after deposition. Sample refractive index (RI), and thickness were measured by VASE ellipsometer. It took approximately 25 minutes to allow the system to warm and for the calibration and sample alignment to be completed. The wavelength range used was 300 to 1200 nm with a step of 10 nm. The incident angle was selected from 55 to 75° with a step of 5°.

5.1.1 General Modeling

After data recording, modeling, the critical part in VASE characterization, was done using the "normal fit" option. The general procedure was to minimize the difference between the observed data (y) and the model prediction (Y) to minimize the Mean Square Error (MSE) which is defined as $MSE = \frac{1}{j}\sum_{i=1}^{j}(y_i - Y_i)^2$. Modeling was done with and without considering surface roughness. Without the roughness model, the "Si-Al_2O_3" layers were considered as shown in Figure 5-1. When modeling with roughness, the "Si-Al_2O_3-surface roughness (srough)" layers were used as shown in Figure 5-2. The SiO_2 layer for native oxide was not used as described in section 4.3. In modeling, optical constants and thickness of the sample are individually selected as measurement variables.

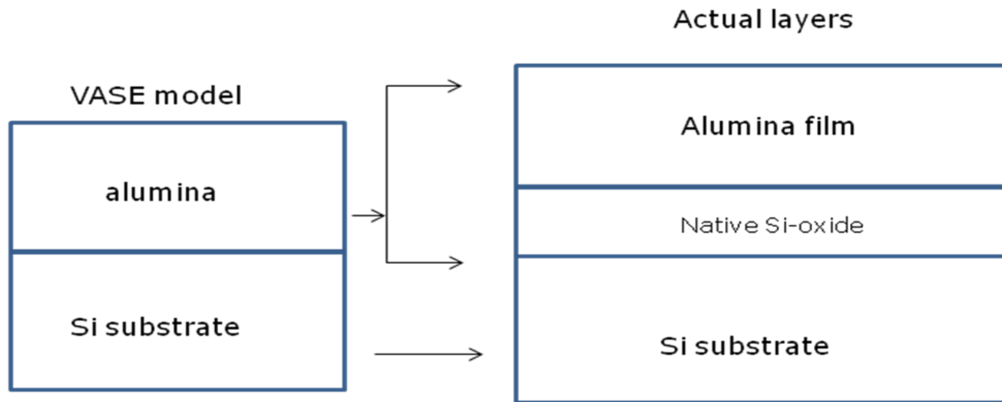

Figure 5-1 VASE model and actual sample layers arrangement without roughness considered

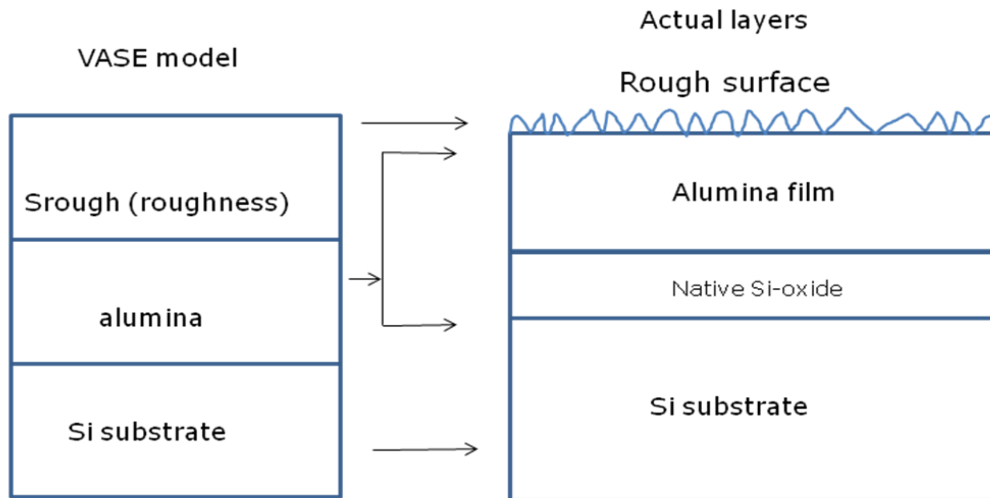

Figure 5-2 VASE model and actual sample layers arrangement with roughness considered

When one quantity is not selected as a measurement variable, the system uses the fixed reference values for that quantity from the system for the corresponding layers used in the modeling. An expected value of film thickness can be put in the model before every run. The surface roughness model mixes 50% surface material with 50% void. The roughness model should be included only if the MSE reduces by ~50% compared to the model without surface roughness. In modeling, using the surface roughness model reduces the MSE value in several cases as shown in Figure 5-3 from general modeling. MSE for both general and Cauchy model were less than 3.05% .

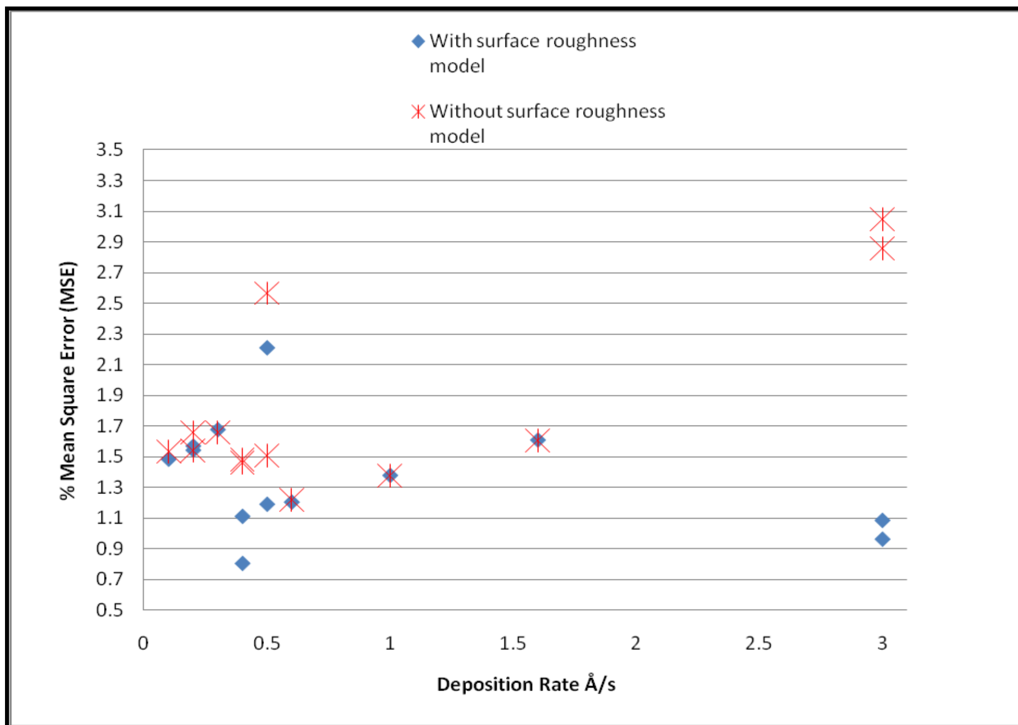

Figure 5-3 MSE comparison between roughness and non-roughness model from general modelling

When samples were measured the following procedure was used. The first layer was Si as the substrate, then Al_2O_3 (with fixed optical constants) with thickness as a variable without any expected thickness value, and then surface roughness as variable. This run gave the film thickness and surface roughness based on the optical constants of the reference values from the software. Then the RI was changed to a variable while keeping both thickness and roughness as variables. The previous thickness reading was used as the expected film thickness input. In the non-roughness model, the same process was followed except there was no roughness layer in the model.

5.1.2 Cauchy Modeling

The refractive index of dielectric materials varies smoothly with wavelength in the transparent (Extinction Coefficient k=0) region and can be expressed by the Cauchy equation, given by-

$$n(\lambda) = A + \frac{B}{\lambda^2} + \frac{C}{\lambda^4} \qquad \text{(5.1)}$$
$$when, k(\lambda) = 0$$

Where A, B, and C are constants having different values for different materials. Constant A sets the index amplitude and B and C give the curve shape. A_{Al2O3} ~1.75 for bulk alumina, B and C are less than 0.1[23]. For Cauchy modeling, the layer modeling was the same as described earlier except that the RI for Al_2O_3 was replaced by a "Cauchy layer". The thickness of both the Cauchy and the srough

layer were kept as variables in first run. In second run, constants A, B, and C and thicknesses were kept as variables. The curves obtained from the Cauchy formula coincide well with the measured curve but are smooth and well defined as shown in Figure 5-4.

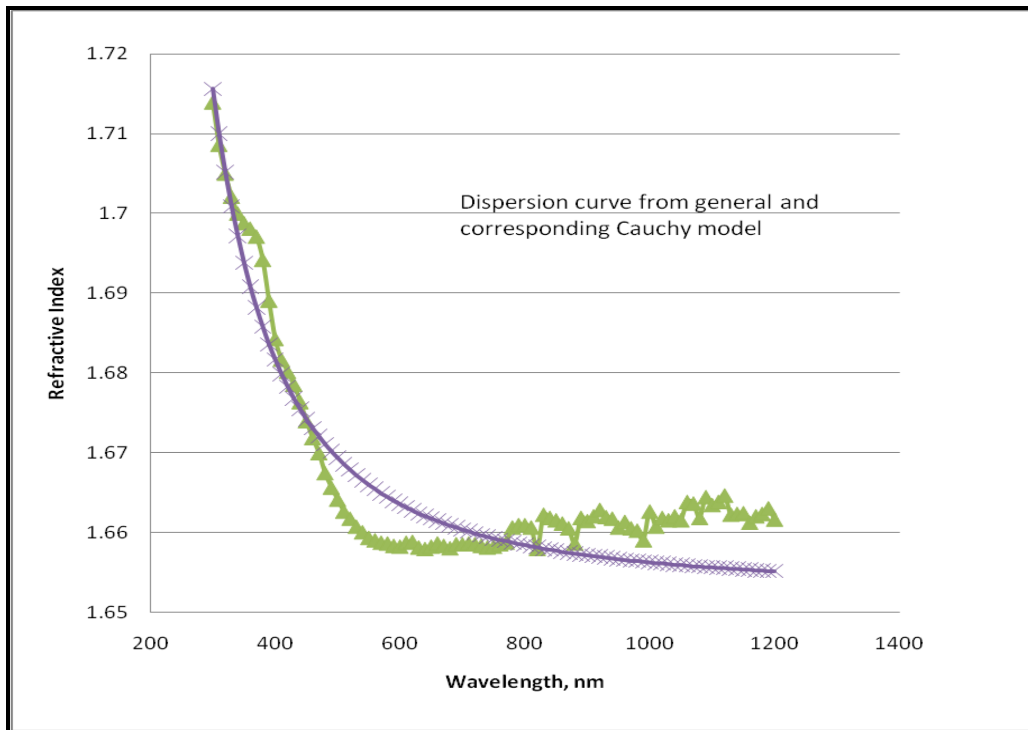

Figure 5-4 Dispersion curve from general and corresponding Cauchy model

Both the general and the Cauchy models, with and without surface roughness, are valid and in this work the general model without roughness was used. In those instances where the Cauchy model and/or models with roughness were used they are so indicated in the figure legend. A comparison of the VASE modeling parameters used for the Al_2O_3 layer (the general model) and the Cauchy layer are summarized in Table 5-1. The thickness measured by VASE general modeling

with and without roughness and crystal monitoring system are summarized in Table 5-2

Table 5-1 VASE Modeling Parameters

Parameters	Al_2O_3 layer	Cauchy layer
Model layers	Si(substrate)-Al_2O_3 Si(substrate)-Al_2O_3-srough	Si(substrate)-Cauchy Si(substrate)-Cauchy-srough
Wavelength range (10 nm steps)	300 – 1200 nm	300 –1200 nm
Angle of incidence	55-75° with 5° steps	55-75° with 5° steps

Table 5-2 Sample Thickness

From VASE with roughness, base + roughness = total, nm	From VASE without roughness, nm	From crystal monitor, nm
30.35+3.00 = 33.35	32.70	30
30.20+2.21 = 32.41	31.94	30
31.98+0.00 = 31.98	31.97	32
33.70+3.86 = 37.56	36.56	35
34.18+4.02 = 38.20	37.1	35

5.2 Influence of Deposition Variables

Several samples were prepared by varying the deposition rate from 0.1 - 3.0 Å/s. Each sample was characterized by VASE. For comparison, RI values at a particular wavelength, 630nm, were plotted against corresponding deposition rate as shown in Figure 5-5.

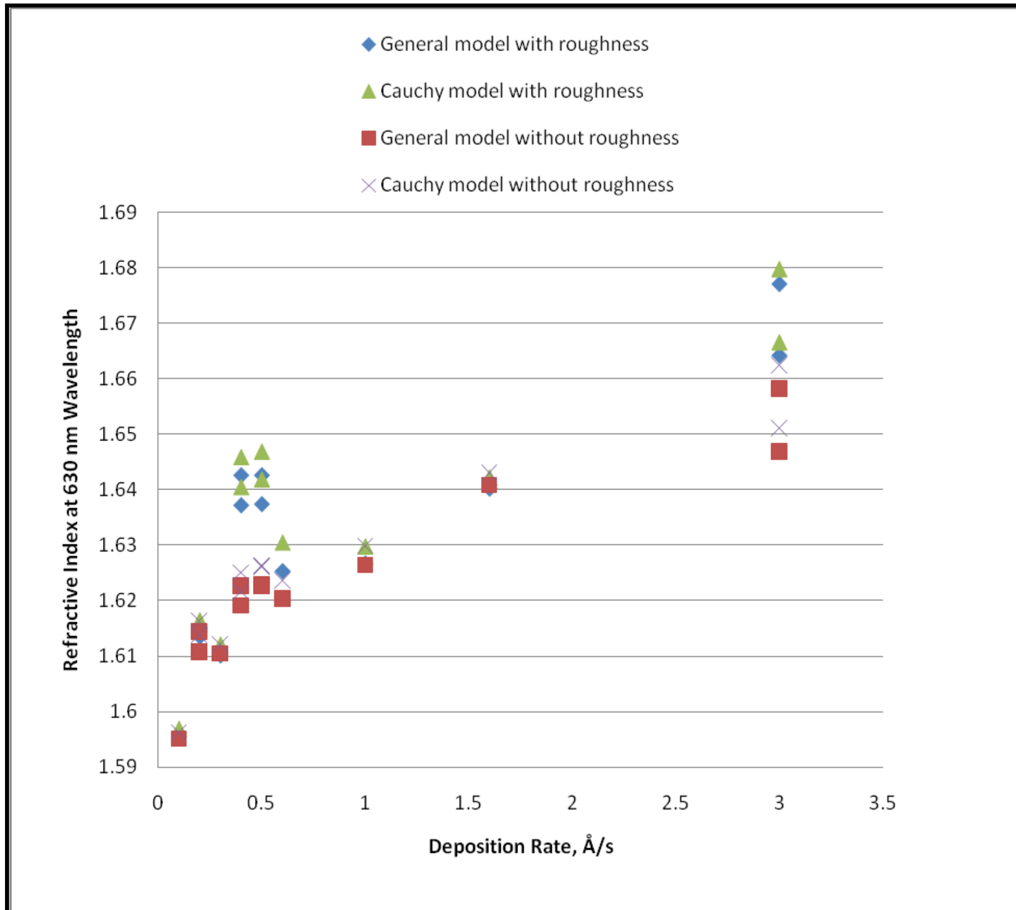

Figure 5-5 Refractive index vs. deposition rate

The RI increases with deposition rate. However, there are some inconsistencies between the data obtained with and without the roughness model at 0.4, 0.5 and 3.0 Å/s. These deposition rate experiments were repeated, keeping all parameters same, and the same RI values were obtained. The reason for this discrepancy is not clear. There is also an increase in RI with deposition rates. This increase may occur for two reasons:

1. In order to increase the deposition rate the electron beam current is increased, with a subsequent increase in energy density and temperature of the melt. This increases the thermal energy, $3/2K_BT$, of the evaporating species as described in section 3.2.2. The kinetic energy of the evaporated species converts into heat upon colliding with substrate increasing the mobility of the deposited species during film growth. As a result a higher density film with higher RI is deposited compared to the film deposited with lower deposition rate. This suggests that RI should increase with deposition rate.

2. Alumina molecules evaporating from the melt dissociate more with increased deposition rate due to the increase in energy density and temperature of the melt. At much higher temperatures, more metallic films are deposited giving higher RI at higher deposition rates.

RI will keep increasing with higher deposition rate if it is due to the dissociation of Al and O_2 and more metallic films deposit. However as more Al_2O_3 dissociates the partial pressure of O_2 in the chamber will increase and start to oxidize the metal in film, so the RI increase would start to level off.

It is evident from Figure 5-5 that when the model is run with roughness, the RI at 0.4, 0.5 and 3.0 Å/s deposition rates are higher than those in the model without roughness. At all of the other deposition rates, the two models coincide. If the roughness, calculated by the roughness model, is plotted versus the deposition rate there doesn't appear to be any relationship between the two variables as shown in Figure 5-6. It is clear from Figure 5-5 that the RI is also higher at the same

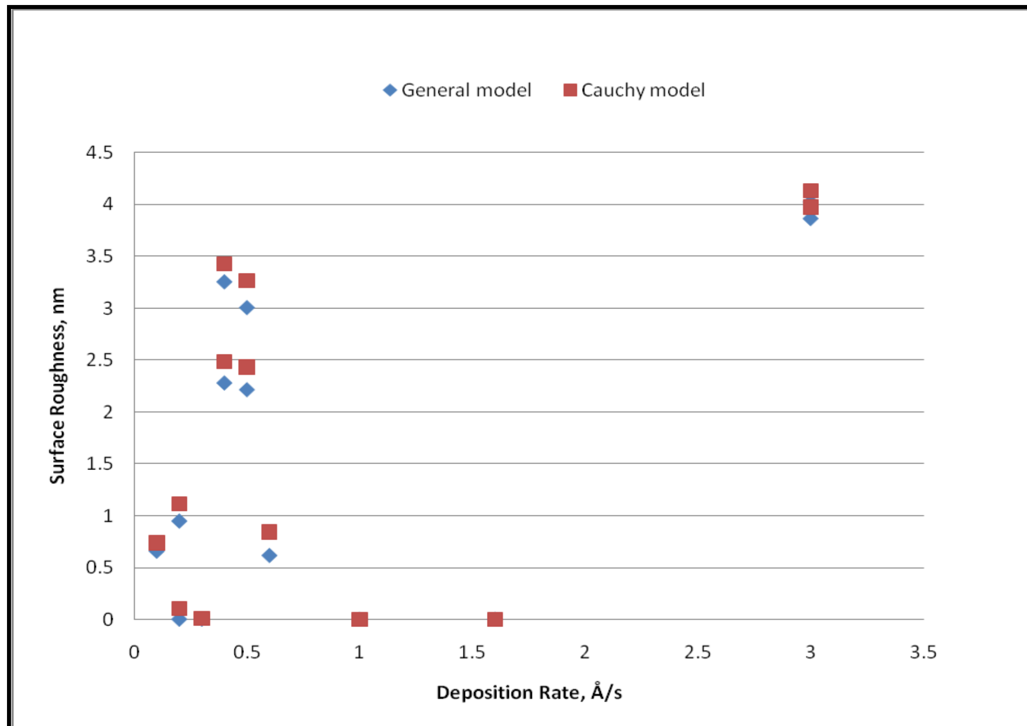

Figure 5-6 Surface roughness vs. deposition rate

deposition rates that give higher roughness values. It appears that higher RI values given by the roughness model are due to the higher roughness. General and Cauchy models were compared with and without roughness fittings. The model without roughness has a much better fit than the roughness model as shown in Figure 5-7.

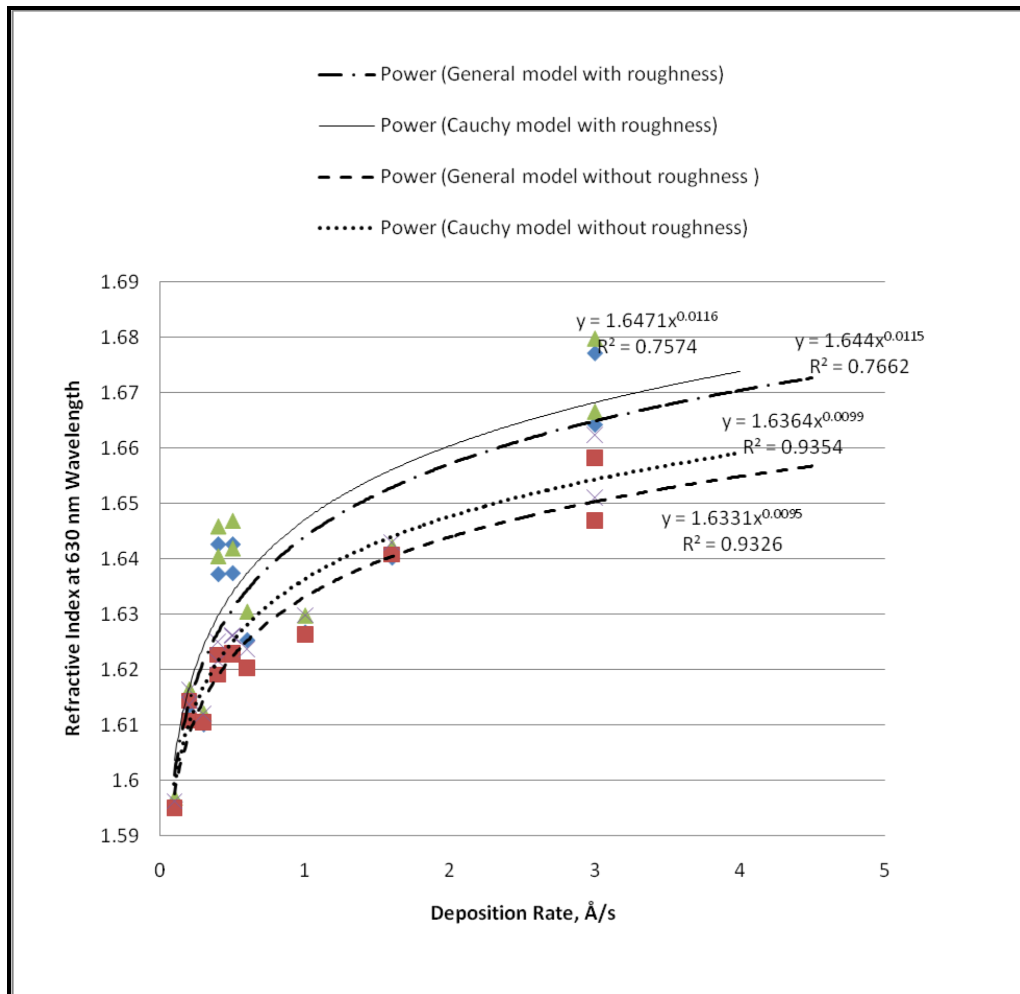

Figure 5-7 Possible trends of refractive index with deposition rate

All of the samples deposited at all of the deposition rates used in these experiments give general dielectric dispersion curves as shown in Figure 5-8. The measured RI values, at higher deposition rates, were higher than previously published values for electron beam deposited alumina thin films (see Figure 2-1).

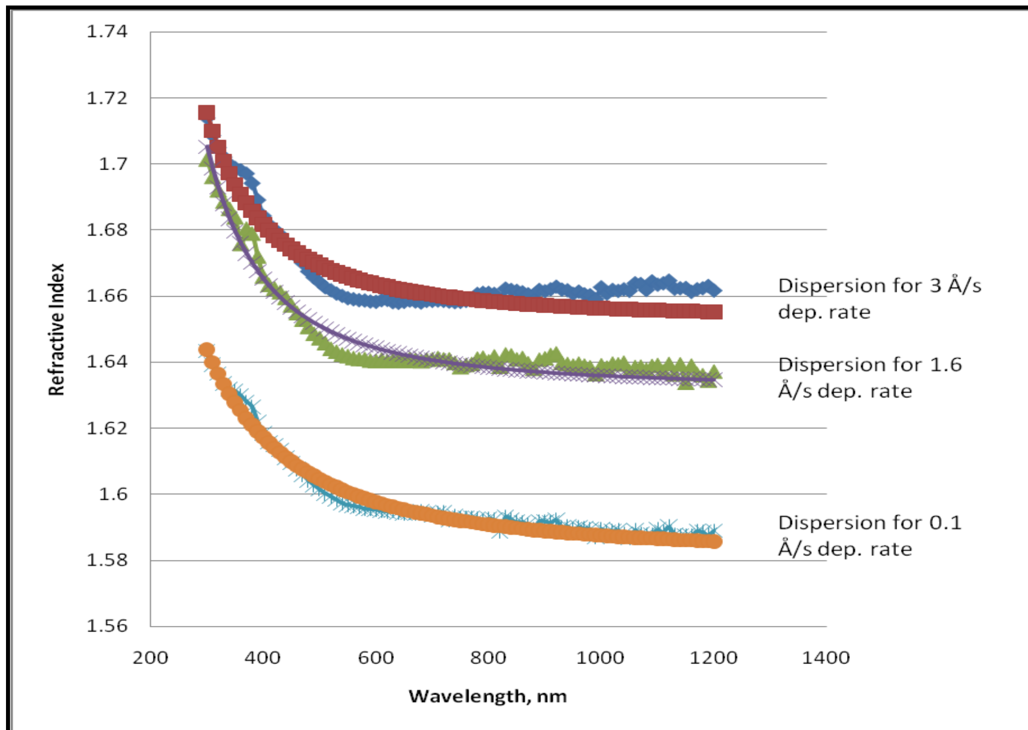

Figure 5-8 Dispersion curves from general model and corresponding Cauchy model at 0.1, 1.6, and 3.0 Å/s deposition rate

These results also compared well with the sapphire reference dispersion curve from the VASE as shown in Figure 5-9. For a pure aluminum, the RI variation with wavelength is quite different than dispersion curve of alumina.

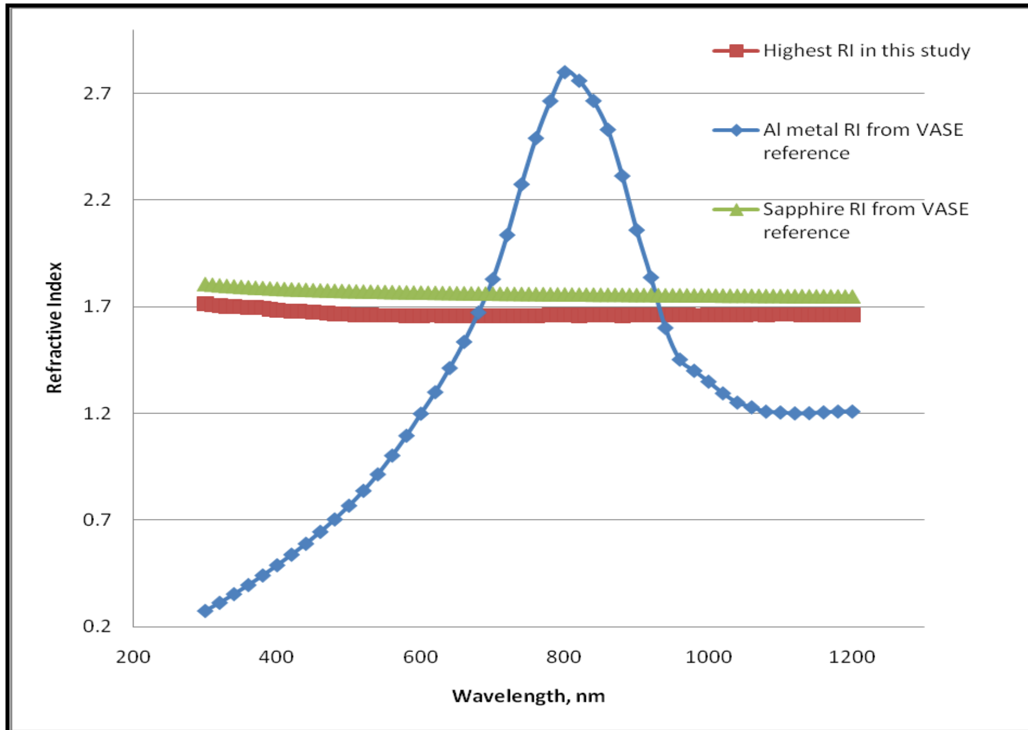

Figure 5-9 Refractive index of Al metal and alumina within 300-1200nm wavelength rage

Experiments were carried out to determine if there was an oxygen deficiency in the films at a lower deposition rate. Samples were deposited with additional oxygen in chamber at 0.2 Å/s deposition rate and were characterized in the VASE. The results are shown in Figure 5-10 which shows the variation of refractive index and surface roughness with supply oxygen in the chamber.

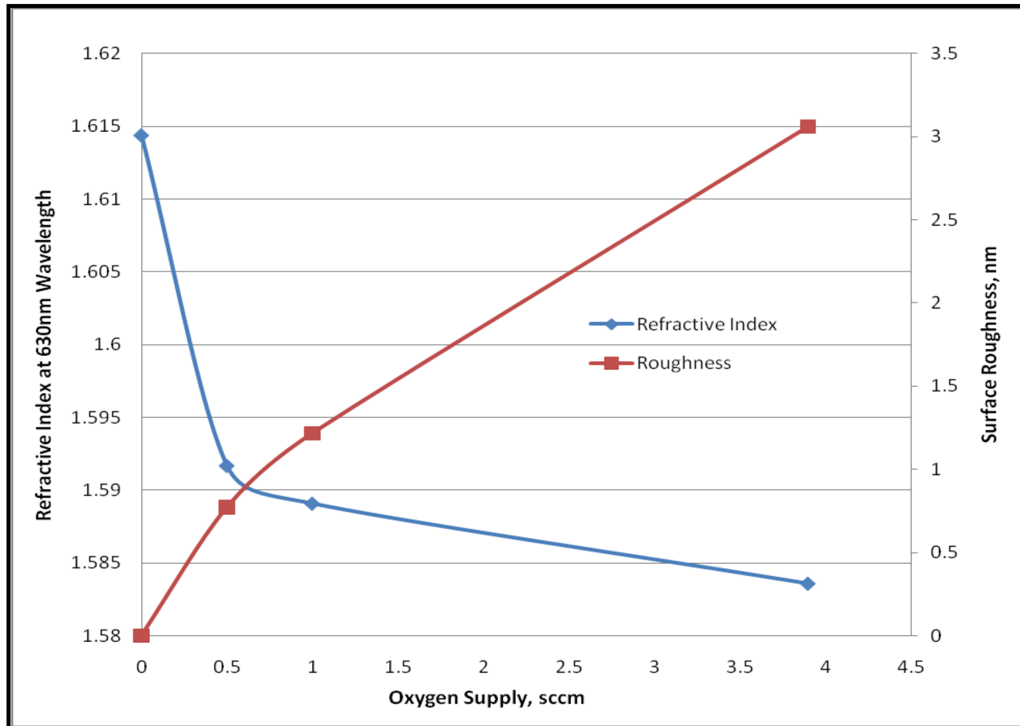

Figure 5-10 Variation of refractive index and surface roughness with additional oxygen in the chamber

As the O_2 supply rate was increased, the surface roughness increased and RI decreased. Nightingle et al [10] also observed the reduction of RI with increased oxygen pressure during ion assisted electron beam deposition. The increase in chamber pressure, due to the oxygen supply, lowers the kinetic energy of the evaporated species and contributes to lower density films. The decrease in RI is more likely due to a decrease in film density with increased chamber pressure. Oxygen will also affect the film as it grows on the substrate because it reduces the mobility of specie on the substrate surface.

The RI of all film samples, deposited with and without additional oxygen, were measured again after exposure to room temperature air for more than 24hrs. The samples exposed to air all had increased RI as shown in Figures 5-11 and 5-12.

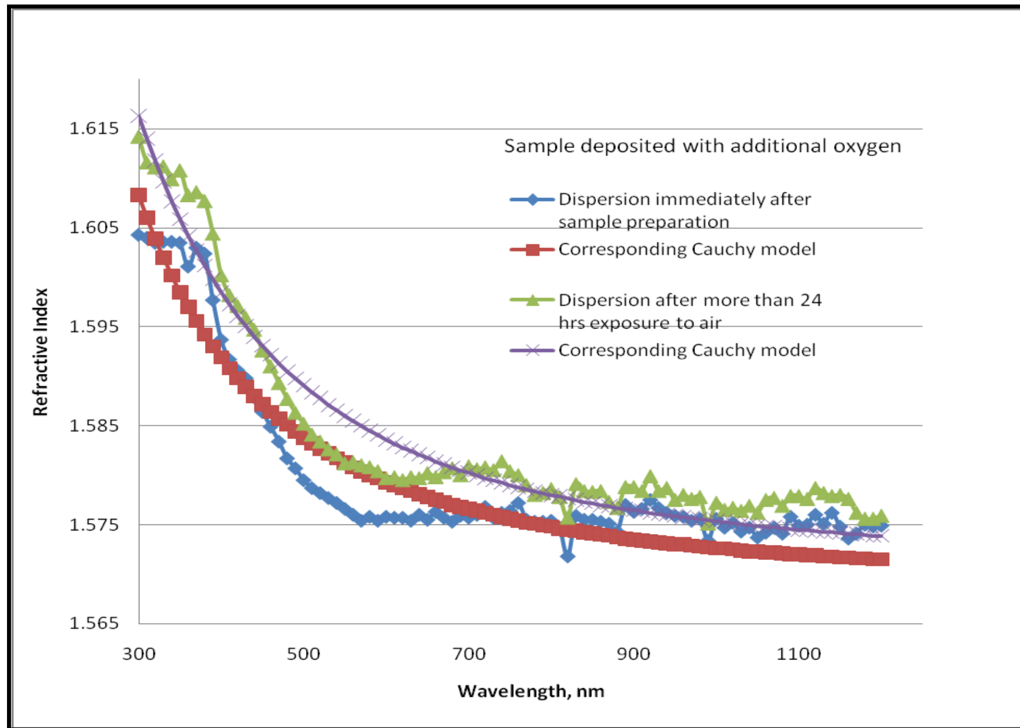

Figure 5-11 Dispersion curve change after exposure to air at room temperature for more than 24 hrs

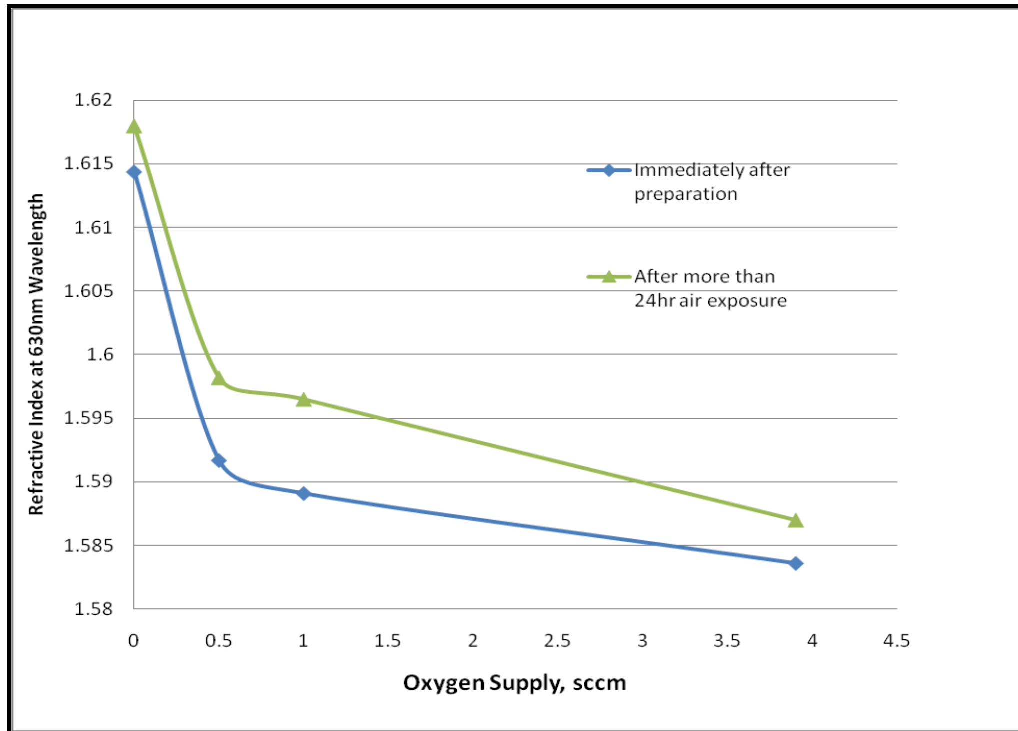

Figure 5-12 Refractive index increase upon exposure to air for samples deposited with additional oxygen in the chamber

The change in RI upon exposure to air may occur due to:

(a) A stoichiometry change where the lack of oxygen in suboxide films are compensated by oxygen from the air

(b) Water vapour fills the void columns of the porous lower density films

(c) Both (a) and (b)

The films deposited with oxygen in the chamber were deposited at a low deposition rate, 0.2 Å/s, and therefore should not have much Al_2O_3 dissociation. Even if there is any dissociation, it would have been supplemented by the additional oxygen in the chamber. Therefore, the film should be stoichiometric and should not change RI upon exposure to air. Since this does not happen, it is clear that films deposited with oxygen supply in the chamber and at lower deposition rate are not lacking oxygen and the reason for the lower RI with oxygen supply is due to lower film density.

Extinction Coefficient k of all the samples were measured within 300-1200 nm wavelength region using the same VASE modeling parameters as summerized in table 5.1. Only general modeling without surface roughness were used. In all cases, k were less than 0.023, which is far less than that of conducting materials in that wavelength region, as expected for the insulating films.

6. CONCLUSIONS AND FUTURE WORK

6.1 Conclusions

In this study, it has been found that the optical quality of ebeam deposited alumina films grown from source alumina depends on the film growth rate. Refractive index increases with increased deposition rate. The increase in RI occurs due to increased film density and Al/O composite ratio as described in section 5.2. It was reported by Kubler et al [13] that homogeneity and therefore electrical properties of the films change with evaporation rate. They also reported inhomogeneous porous films would give different electrical properties in different regions of the films. It was also reported by Yoon et al [11] that the refractive index changes with film density and Al/O ratio for alumina deposited from source Al and oxygen plasma reaction. They concluded that a higher value of RI in alumina films occurs due to the aluminum-rich films. Matolin et al [12] reported that stoichiometry of the films depend on the evaporation rate that corresponds to ebeam emission power. They have found Al rich alumina films at higher evaporation rate and metallic films at much higher evaporation rates. Al rich films come from increased dissociation of compounds with increased evaporation temperature. From the Figure 5-8, it is observed that RI dispersion curve for highest deposition rate still behaves like dielectric material. It can be concluded that both film density and increased Al/O ratio contribute to the increase in RI with deposition

rate. It is noted that the highest measured RI in this study is higher than any previous RI published deposited by ebeam evaporation.

From Figure 5-7, it is noticed that RI increase with evaporation rate for alumina films is following a power curve. However, RI is not expected to keep increasing with evaporation rate as the chamber always has a partial pressure of oxygen and water.

Samples deposited with oxygen supplied to chamber at low deposition rate are not expected to have suboxide forms. From Figure 5-10 , it can be concluded that films deposited with increased oxygen supply have lower density that decreases RI. The decrease in density and RI with increased oxygen supply was observed by Nightingle et al [10] during ion assisted electron beam deposition. All the samples deposited with and without oxygen supply have increased RI upon exposure to air. This change is mostly due to water filling the void columns of the low density films.

6.2 Future work

Further investigations are required to understand the trend line of RI increase with increased deposition rate. Film composition characterization techniques need to be used to understand how stoichiometry of the films changes with increased deposition rate. Samples deposited without oxygen supply should be studied to see if suboxide molecules become stable upon exposure to air. Stoichiometry and

insulating properties of the alumina samples need to be verified. The change in films quality with deposition rate in ebeam deposition should also be investigated for metal film deposition where metal film quality could change with kinetics of the evaporated species. A simple technique could be to measure the variation of resistivity of metal films with ebeam deposition rate with increased ebeam current.

References

1. G. A. Parks, “Free energies of formation and aqueous solubilities of aluminum hydroxides and oxide hydroxides at 25°C”, American Mineralogist, Vol. 57, pp. 1163-1189, 1972

2. I. H. Malitson, “Refraction and dispersion of synthetic sapphire”, Journal of the Optical Society of America. Vol. 52, No.12, pp. 1377-1379, 1962

3. T. S. Eriksson, A. Hjortsberg, G. A. Niklasson, and C. G. Granqvist, “Infrared optical properties of evaporated alumina films”, Applied Optics, Vol. 20, No. 15, pp. 2742-2746, 1981

4. B. Tiwari, J. A. Bean, G Szakmany, G. H. Bernstein, P. Fay, and W. Porod, “Controlled etching and regrowth of tunnel oxide for antenna-coupled metal-oxide-metal diodes.”, Journal of Vacuum Science and Technology B, Vol. 27 (5), pp. 2153- 2160, 2009

5. I. Shimizu, Y. Setsuhara, S. Miyake, M. Kumagai, K. Ogata, M. Kohata, K. Yamaguchi, “Preparation of aluminum oxide films by ion beam assisted Deposition”, Surface and Coatings Technology, Vol. 131, pp. 187-191, 2000

6. J. Gallup, “The transformation of aluminum oxide from the beta to the alpha form”, RCA Radiotron Division, RCA Manufacturing Co, Inc., Harrison, New Jersey

7. K. Ogata, K. Yamaguchi, S. Kiyama, H. Hirano, S. Shimizu, M. Kohata, T. Miyano, Y. Setsuhara, and S. Miyake, “Synthesis of aluminum oxide thin films by ion beam and vapour deposition technology”, Nuclear Instruments and Methods in Physics Research, B 80/81, pp.1423-1426, 1993

8. R.F. Bunshah and A. C. Raghuram, “Activated Reactive Evaporatin Process for High Rate Deposition of Compounds”, J. Vac. Sci. Technol. Vol. 9, No. 6, pp.1385-1388, 1972

9. E. M. DaSilva and P. White,“Electrical properties of evaporated aluminum oxide films”, Journal of the Electrochemical Society, Vol. 109, No.1, pp. 12-15, 1962

10. J. R. Nightingale, T. Cornell, P. Samudrala, P. Poloju, L. A. Hornak, and D. Korakakis “Reactive deposition of dielectrics by ion beam assisted e-beam evaporation”, Mater. Res. Soc. Symp. Proc., Vol. 983, 2007

11. J. S. Yoon, G. F. Potwin, H. J. Doerr, C. V. Deshpanday, and R. F. Bunshah, “ Fabrication of aluminum oxide films with high deposition rates using the activated reactive evaporation technique”, Surface and Coatings Technology, Vol. 43-44, pp. 213-222, 1990.

12. V. Matolin, V. Nehasil, L. Bideux, C. Robert, and B. Gruzza, “Vacuum evaporation of thin alumina layers”, Thin Solid Films, Vol. 289, pp. 295-299, 1996.

13. W. Kubler, “Properties of Al_2O_3 thin films prepared by ion-assisted evaporation”, Thin Solid Films, Vol. 199, pp. 247-257, 1991.

14. J. Saraie, S. Goto, Y. Kitao, and Y. Yodogawa, “High quality Al_2O_3 thin films prepared by a novel two-step evaporation process”, J. of the Electrochemical Society: Solid-State Science and Technology, Vol. 134, No. 11, pp. 2805-2809, 1987.

15. P.V. Patil, D. M. Bendale, R. K. Puri, and V. Puri, “Refractive index and adhesion of Al_2O_3 thin films obtained from different processes – a comparative study”, Thin Solid Films, Vol. 288, pp. 120-124, 1996.

16. J. T. Cox, H. Hass, and J. B. Ramsey, “ Improved dielectric films for multilayer coatings and mirror protection”, J. Phys. (Paris) 25, pp. 250-254, 1964.

17. D. Hoffman, and D. Leibowitz, “Al_2O_3 films prepared by electron-beam evaporation of hot-pressed Al_2O_3 in oxygen ambient”, Journal of Vacuum Science and Technology, Vol. 8, No.1, pp. 107-111, 1971.

18. C.W. Hanks, “Electron beam furnace with low beam source”. US patent number 31777535. April 13, 1965

19. K.S. Sree Harsha, Principles of vapour deposition of thin films first edition, Elsevier Ltd, UK, 2006.

20. Instruction Manual of FTM7 Film Thickness Monitor, Edwards High Vacuum International, UK

21. http://www.lesker.com/newweb/deposition_materials/depositionmaterials_CertForm.cfm?partno=EVMALO-1220K, on Nov 25, 2010.

22. VASE brochure 2007, J.A Woollam Co., Inc., 2007.

23. Ron Synowicki and Neha Singh, J. A. Woollam Co., Inc., 2007.